AGU PUBLICATIONS

JGR

Journal of Geophysical Research: Atmospheres

RESEARCH ARTICLE
10.1002/2017JD027093

Key Points:
- The temporal variability of vertical structure of TTL cirrus cloud fraction can be well explained by the vertical temperature gradient
- The TTL cirrus at a given altitude is best correlated with the temperature at a higher altitude, and this displacement decreases with height
- The ENSO and QBO are the leading factors in controlling the spatial variability of the TTL cirrus clouds and temperatures

Correspondence to:
H.-H. Tseng,
hhtseng@uw.edu

Citation:
Tseng, H.-H., & Fu, Q. (2017). Temperature control of the variability of tropical tropopause layer cirrus clouds. *Journal of Geophysical Research: Atmospheres*, *122*, 11,062–11,075. https://doi.org/10.1002/2017JD027093

Received 8 MAY 2017
Accepted 29 SEP 2017
Accepted article online 5 OCT 2017
Published online 23 OCT 2017

Temperature Control of the Variability of Tropical Tropopause Layer Cirrus Clouds

Hsiu-Hui Tseng[1] and **Qiang Fu**[1]

[1]Department of Atmospheric Sciences, University of Washington, Seattle, WA, USA

Abstract This study examines the temperature control of variability of tropical tropopause layer (TTL) cirrus clouds (i.e., clouds with bases higher than 14.5 km) by using 8 years (2006–2014) of observations from the Cloud-Aerosol Lidar and Infrared Pathfinder Satellite Observations (CALIPSO) and Constellation Observing System for Meteorology, Ionosphere, and Climate (COSMIC). It is found that the temporal variability of vertical structure of TTL cirrus cloud fraction averaged between 15°N and 15°S can be well explained by the vertical temperature gradient below ~17.5 km but by the local temperature above for both seasonal and interannual time scales. It is also found that the TTL cirrus cloud fraction at a given altitude is best correlated with the temperature at a higher altitude and this vertical displacement increases with a decrease of the cirrus altitude. It is shown that the TTL cirrus cloud fractions at all altitudes are significantly correlated with tropical cold point tropopause (CPT) temperature. The plausible mechanisms that might be responsible for the observed relations between TTL cirrus fraction and temperature-based variables are discussed, which include ice particle sediments, cooling associated with wave propagations, change of atmospheric stability, and vertical gradient of water vapor mixing ratio. We further examine the spatial covariability of TTL total cirrus cloud fraction and CPT temperature for the interannual time scale. It is found that the El Niño–Southern Oscillation and quasi-biennial oscillation are the leading factors in controlling the spatial variability of the TTL cirrus clouds and temperatures.

1. Introduction

The transition from the tropical troposphere to the stratosphere is generally a layer that extends several kilometers vertically instead of a sharp boundary (e.g., Fueglistaler et al., 2009; Highwood & Hoskins, 1998). This layer is termed the tropical tropopause layer (TTL), which is from about 14.5 to 18.5 km (Alcala & Dessler, 2002; Folkins et al., 1999; Fu et al., 2007; Gettelman et al., 2004; Gettelman & Forster, 2002; Holton & Gettelman, 2001; Sherwood & Dessler, 2000). In this study, we define the TTL clouds as clouds with bases higher than 14.5 km (Tseng & Fu, 2017).

It has been suggested that radiative heating rates of the TTL clouds play an important role in enhancing the upwelling in the TTL (Corti et al., 2006, 2005; Lin et al., 2013; Yang et al., 2010) in addition to the TTL clouds being an indicator of the dehydration processes. The TTL clouds are thus of interest because of not only their influence on the radiative energy budget (e.g., Comstock et al., 2002; Fueglistaler & Fu, 2006; Jensen et al., 1996) but also their significant implications for stratospheric composition and ultimately on surface climate (Bethan et al., 1996; Brasseur & Solomon, 2006; Solomon et al., 2010; Tuck et al., 1997). Therefore, it is essential to understand the processes governing the distributions and variability of the TTL clouds.

It is well recognized that air enters the stratosphere primarily through upwelling in the tropics (Brewer, 1949; Dobson, 1956; Holton et al., 1995). The TTL temperatures control the tropical lower stratospheric water vapor amount through the dehydration process (e.g., Brewer, 1949; Ding & Fu, 2017; Fueglistaler et al., 2009; Fueglistaler & Haynes, 2005), and thus, the temperature is a critical factor in influencing the TTL cloud formation by bringing air to saturation. By analyzing satellite data, recent studies have shown that annual variations of the TTL clouds and tropical tropopause temperatures are strongly inversely correlated both temporally and spatially (Fu, 2013; Tseng & Fu, 2017; Virts et al., 2010). On the other hand, the variability of the TTL temperature is largely caused by a complex combination of the stratospheric quasi-biennial oscillation (QBO), tropospheric convective processes in the tropics, and the Brewer-Dobson circulation (BDC) driven by midlatitude and subtropical atmospheric waves (e.g., Ding & Fu,

2017). Randel et al. (2002) found that the variation in vertical velocity is capable of significantly changing temperatures in the tropical tropopause region, indicating that the TTL temperature variability is largely controlled by mechanically driven upwelling in the upper troposphere and lower stratosphere. It is evident that the TTL temperature variability is modulated by both equatorial and extratropical waves (Grise & Thompson, 2013; Held & Hoskins, 1985; Kerr-Munslow & Norton, 2006; Norton, 2006). Since there is strong coupling between temperature and cloud in the TTL, the TTL clouds can also be modulated by these large-scale circulations and wave activities. Li and Thompson (2013) and Fu (2013) suggest that the BDC plays an important role in the seasonal cycle of TTL cirrus. Virts and Wallace (2010) demonstrate that the Madden-Julian Oscillation (MJO) modulates tropopause temperature and TTL cloud on intraseasonal scales. Li and Thompson (2013) show a significant linkage between the BDC and zonal mean TTL clouds on month-to-month time scales during the Northern Hemisphere (NH) winter months (October–March) based on anomalous data. Davis et al. (2013) examine the interannual variability of TTL clouds in responses to the El Niño–Southern Oscillation (ENSO), BDC, and QBO.

The objective of this study is to examine the temperature control of the variability of the TTL clouds on both seasonal and interannual time scales. We use 8 years (2006–2014) of the Cloud-Aerosol Lidar and Infrared Pathfinder Satellite Observations (CALIPSO) cloud data and Constellation Observing System for Meteorology, Ionosphere, and Climate (COSMIC) temperature measurement. We found that the temporal variability of vertical structure of TTL cirrus cloud fraction averaged over the deep tropics (15°N–15°S) can be better explained by the vertical temperature gradient than local temperature, which complements previous studies that suggest the TTL clouds occurs as a result of cold temperature anomaly (e.g., Boehm and Verlinde, 2000; Taylor et al., 2011). It is also shown that the TTL cirrus cloud fraction at a given altitude is always best correlated with the temperature at a higher altitude and this vertical displacement increases with a decrease of cirrus height. It is shown that the TTL cirrus at all altitudes is significantly correlated with tropical cold point tropopause temperature at the 95% confidence level.

We further examine the spatial covariability of total TTL cirrus fraction and cold point tropopause temperature over the entire tropics (30°N–30°S) by using the maximum covariance analysis (MCA) and explore their relations to the large-scale dynamical variability on the interannual time scale. It is shown that the ENSO and QBO, which closely correspond to the MCA first and second modes, respectively, are the main factors in controlling the spatial variability of the TTL cirrus clouds and temperatures. It is also shown that the MJO is significantly correlated with the MCA third mode but the BDC is not significantly related to any of the first three MCA modes. These results except the leading role of ENSO in determining the TTL cloud and temperature spatial variability are somewhat different from Davis et al. (2013). Davis et al. (2013) showed that the BDC plays an important role in determining the spatial distribution of TTL clouds but QBO does not (they did not consider the role of MJO). This is mainly because Davis et al. (2013) used the total heating rate anomaly at 82 hPa as a measure of the BDC upwelling, which includes the variability due to QBO (Yang et al., 2008). Different from Davis et al. (2013), this study uses the BDC index that is a measure of wave propagating vertically into the extratropical stratosphere. This index thus does not include the QBO contribution so that we could better understand their relative role in controlling the spatial variabilities of TTL cirrus and temperatures. We also show that the variability of tropical mean TTL cirrus and temperature is dominated by both QBO and BDC signals (Davis et al. (2013) reached the same conclusion but for different reason as will be discussed later in this paper). This is because the spatial positive and negative signals associated with ENSO and MJO are largely canceled out in the tropical zonal mean analysis. Davis et al. (2013) also notice the spatial positive and negative signals associated with ENSO.

Virts and Wallace (2010) investigated annual, interannual and intraseasonal variability of TTL cirrus clouds. They found that for the annual cycle, the TTL cirrus clouds are largely equatorially symmetric, with a maximum in the boreal winter throughout most of the tropics. They showed that ENSO signature in TTL cirrus is marked by a zonal shift of the peak cloudiness toward the central Pacific during El Niño and toward the Maritime Continent during La Niña. The present work complements the study by Virts and Wallace (2010) by examining the relation between the TTL cirrus and temperature-based variables as a function of height in both seasonal and interannual variations, and investigating the role of ENSO, MJO, QBO, and BDC in the TTL cirrus interannual variability instead only the role of ENSO. Note that Virts et al. (2010) and Virts and Wallace (2010, 2014) examine the role of MJO on the intraseasonal (not interannual) variability of TTL cirrus clouds.

This paper is organized as follows. Section 2 describes the data used. Section 3 presents the temporal and vertical variability of the TTL cloud fraction and temperature-based variables averaged over 15°S–15°N, quantifies their relation, and discusses the underlying mechanisms. Section 4 shows the spatial covariability between the TTL total cloud fraction and tropopause temperature over the entire tropics and their relations to the large-scale dynamical variability. The discussion and conclusion are given in section 5.

2. Data

2.1. CALIPSO

CALIPSO satellite was launched in April 2006 to a Sun-synchronous, 98.2° inclination polar orbit at an altitude of 705 km as part of the A-train constellation of satellites (Winker et al., 2010). The constellation repeats the cycle every 16 days with local equator crossing times of nearly 01:30 h and 13:30 h (Winker et al., 2009). The main instrument on board CALIPSO is the Cloud-Aerosol Lidar with Orthogonal Polarization (CALIOP), which is a dual wavelength (532 nm and 1,064 nm) polarization sensitive lidar. CALIOP provides vertical profiles of clouds and aerosols and is capable of detecting clouds with optical depth of 0.01 or less. Using a selective iterative boundary locator algorithm (Vaughan et al., 2009), cloud and aerosol layers are identified from lidar backscatter profiles. In this study, we use the CALIPSO level 2 version 3 5 km cloud and aerosol layer products, which have a vertical resolution of 30 m from the surface to 8.2 km and 60 m from 8.2 km to 20.2 km. The clouds included in the aerosol layer product as so-called "stratospheric features" are considered here by separating clouds from aerosols following Tseng and Fu (2017). We only consider more reliable nighttime measurements because the detection of layers during the daytime has less signal-to-noise ratio for lidar due to solar background noise.

2.2. COSMIC/FORMOSAT-3 Data

The COSMIC satellite mission was launched in April 2006 to a circular, 72° inclination orbit at a 512 km altitude (Anthes et al., 2008). The system includes six identical microsatellites equipped with Global Positioning System (GPS) radio occultation receiver that is able to measure the phase delay of radio wave signals as they are occulted by the Earth's atmosphere. Bending angles and refractivity vertical profiles are then derived from the phase delay (Kuo et al., 2004). The retrieval details of vertical temperature profiles from the bending angle and refractivity profiles are described by Kursinski et al. (1997). The COSMIC has a vertical resolution of ~1 km in the TTL (Kuo et al., 2004; Kursinski et al., 1997). In the upper troposphere and lower stratosphere region, the averaged GPS radio occultation temperature profiles have high accuracies ($<$0.1 K) (Anthes et al., 2008; Hajj et al., 2004; Kursinski et al., 1997). Validation results show that COSMIC is in good agreement with radiosonde data (He et al., 2009; Kuo et al., 2004; Son et al., 2011; Sun et al., 2010). Here we use the COSMIC level 2 temperature product within the TTL where water vapor has little impact on the temperature retrievals.

2.3. ENSO/QBO/BDC/MJO Indices

In this study, we use several large-scale indices to examine the dominant dynamic forcing that impacts the variability of temperature and cloud within the TTL on the interannual time scale. The ENSO index used here is the NOAA Climate Prediction Center Ocean Niño index, which is 3 month running mean of ERSST.v4 SST anomalies in the Niño 3.4 region (5°N–5°S, 120°–170°W). For the QBO index, we used the normalized zonal wind at 30 hPa from the observations of Singapore radiosonde stations. Following Lin et al. (2009), Ueyama and Wallace (2010), and Li and Thompson (2013), the BDC index is here defined as the 3 month mean area-weighted eddy heat flux at 100 hPa averaged over latitudes from 30° to 90° for both hemisphere, which is a measure of the upward propagating wave activity. We calculate the eddy heat flux from the 6-hourly ERA-interim reanalysis data (Dee et al., 2011). The 3 month mean is calculated by averaging the given month and two previous months since the wave activity in the previous 2 months can also contribute to the dynamical heating in the current month (Hu & Tung, 2002). The MJO index used here is the velocity potential MJO index. It is calculated in the same way as the all-seasonal real-time multivariate MJO index (Wheeler & Hendon, 2004) except using the 200 hPa velocity potential instead of outgoing longwave radiation along with zonal wind in a combined empirical orthogonal function (EOF) (Ventrice et al., 2013). The MJO monthly mean index is obtained by averaging the daily data.

3. Temporal and Vertical Variability of the TTL Cloud and Temperature Averaged Over 15°N–15°S

3.1. Temporal and Vertical Variability

The TTL cirrus cloud fraction is calculated from the CALIPSO data for clouds with bases higher than 14.5 km on a 2.5° latitude × 2.5° longitude grid for every 100 m vertically and is then averaged over 15°S–15°N. This is done for each month for the period from June 2006 to April 2014. The temperature from the COSMIC GPS data is analyzed in the same way. Figure 1 shows the climatological annual mean vertical profiles of (a) temperature and vertical temperature gradient from COSMIC and (b) TTL cloud fraction from CALIPSO. The climatological annual mean here is the average of all the monthly profiles from June 2006 to April 2014. We present the vertical temperature gradient since its variability is very relevant to that of the TTL clouds as shown later. The cold point tropopause from the mean temperature profile and thus the zero vertical-temperature-gradient height are located at 17 km (Figure 1a), while the TTL clouds have the highest occurrence at 16 km (Figure 1b). Figures 2 and 3 show the corresponding vertical profiles of standard deviation in temperature, vertical temperature gradient and TTL cloud fraction due to seasonal and interannual variability, respectively. The maximum standard deviation of temperature is located at ~18 km for the seasonal variations but above 20 km for interannual variability (Randel & Wu, 2015). Both vertical temperature gradient and TTL cloud fraction have the maximum standard deviation at ~17 km for both seasonal and interannual variations. It is also noted that for cloud fraction, temperature, and vertical temperature gradient, the standard deviations of the interannual variability are only about half of seasonal one.

The seasonal variation of vertical structure of temperature (T^*) from the COSMIC measurement is shown in Figure 4a, which is the climatology of seasonal cycle after removing the annual mean values in Figure 1. The prominent seasonal variability in the upper TTL temperature, which is coldest in January–February and warmest in July–August, is caused by the annual cycle of the BDC (e.g., Yulaeva et al., 1994). The annual cycle of the BDC is partly driven by the seasonal differences in extratropical planetary wave activities that tend to be largest in the winter and spring seasons in each hemisphere but relatively larger in the Northern Hemisphere, leading to an annual cycle in the total wave activities (Holton et al., 1995; Rosenhof, 1995; Ueyama & Wallace, 2010). Recent studies suggest that the tropical and subtropical wave activities also play an important role in governing the annual cycle of TTL temperatures (Norton, 2006; Randel et al., 2008; Kim, Randel, et al., 2016). The seasonal variability of vertical structure of the TTL cloud fraction (CF*) from the CALIPSO observation is shown in Figure 4b, which is superimposed by the T^* contours from Figure 4a. The temporal phases of the T^* and CF* clearly coincide with each other: the lower (higher) CF* corresponds to a warmer (colder) T^* in boreal summer and early autumn (winter and early spring). However, we note that there is a vertical displacement between these two variables: the maximum (minimum) CF* occur below the minimum (maximum) T^* (i.e., CF* at a given altitude is more coherent with T^* at a higher altitude instead of at the same vertical level).

Figure 4c shows the seasonal variability of vertical structure of the vertical temperature gradient (dT^*/dz) derived from COSMIC temperature measurement. At a given level, dT^*/dz is obtained from the difference between the temperature 100 m above and 100 m below divided by 200 m. The dT^*/dz has strong seasonal variability and the maximum variability occurs around the tropopause (also see Figure 2a). The dT^*/dz has the maximum positive value near the mean tropopause in boreal summer but maximum negative value in boreal winter. Figure 4d is the same as Figure 4b but with dT^*/dz contours from Figure 4c superimposed. It is shown that the CF* and dT^*/dz coincide well with each other both temporally and vertically: A positive dT^*/dz corresponds a negative CF*, while a negative dT^*/dz corresponds a positive CF*.

Figure 5 is the same as Figure 4 but for interannual variability by deseasonalizing the data. The vertical structure of monthly temperature anomalies (T') from the COSMIC is shown in Figure 5a. The vertical structure of the TTL cloud fraction anomalies (CF′) from the CALIPSO are shown in Figure 5b with the superimposed T' contours. The temporal phases of these two variables are clearly coherent, with cold anomalies coincide with positive CF′ and warm anomalies coincide with negative CF′. Similar to the seasonal variability (Figure 4b), there is a vertical displacement between the T' and CF′ (Figure 5b), that is, the CF′ at a given altitude is more coherent with T' at a higher altitude. Figure 5c shows the vertical structure of the vertical temperature gradient anomalies (dT'/dz). Figures 5a and 5c indicate that the T' and dT'/dz exhibit the maximum variability above and near the tropopause, respectively (also see Figure 3a), although they have similar temporal phases.

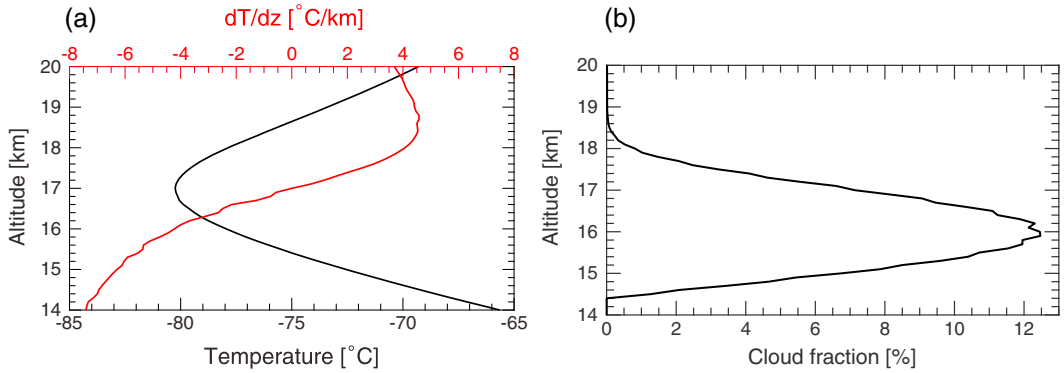

Figure 1. The climatological annual mean vertical profiles of (a) temperature (black line) and vertical temperature gradient (red line) from the COSMIC and (b) TTL cloud fraction from the CALIPSO, averaged over 15°S–15°N from June 2006 to April 2014.

Figure 5d shows the CF′ superimposed by the dT'/dz contours from Figure 5c. It is indicated that CF′ is highly coherent with dT'/dz both temporally and vertically: A positive (negative) CF′ matches well with a negative (positive) dT'/dz. Overall, the temporal and vertical variations of the TTL cloud fraction averaged over 15°S–15°N can be well explained by the vertical temperature gradient on both seasonal and interannual time scales (Figures 4 and 5).

We further analyze the conditions in terms of variability of both temperature and vertical temperature gradient, which favor the positive or negative TTL cloud fraction. Table 1 shows the occurrence frequency under four conditions based on the sign of variability in temperature and vertical temperature gradient for positive and negative TTL cloud fraction variability on both seasonal and interannual time scales. It is shown that negative temperature variability along with negative vertical temperature gradient variability is most favorable for positive TTL cloud fraction variability, while positive temperature variability along with positive vertical temperature gradient variability is least favorable. For negative TTL cloud fraction variability, negative temperature variability along with negative vertical temperature gradient variability is least favorable, while positive temperature variability along with positive vertical temperature gradient variability is most favorable. Furthermore, positive temperature variability along with negative vertical temperature gradient variability is more favorable than negative temperature variability along with positive vertical temperature gradient variability for positive TTL cloud fraction variability. On the other hand, positive temperature variability along with negative vertical temperature gradient variability is less favorable than negative temperature variability along with positive vertical temperature gradient variability for negative TTL cloud fraction variability. Table 1 suggests that at a given level vertical temperature gradient variability is more important than temperature variability itself in controlling the TTL cloud fraction variability, which is consistent with results in Figures 4 and 5. A recent aircraft observational study (Kim, Alexander et al., 2016) also indicated that the vertical temperature gradient is more important to determine TTL cloud occurrence.

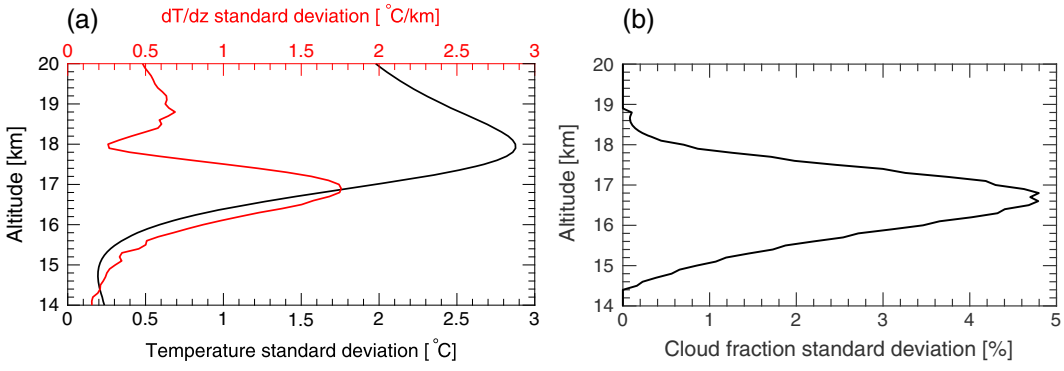

Figure 2. Vertical profiles of standard deviation in (a) temperature (black line) and vertical temperature gradient (red line) and (b) TTL cloud fraction due to the mean seasonal variation for June 2006–April 2014, averaged over 15°S–15°N.

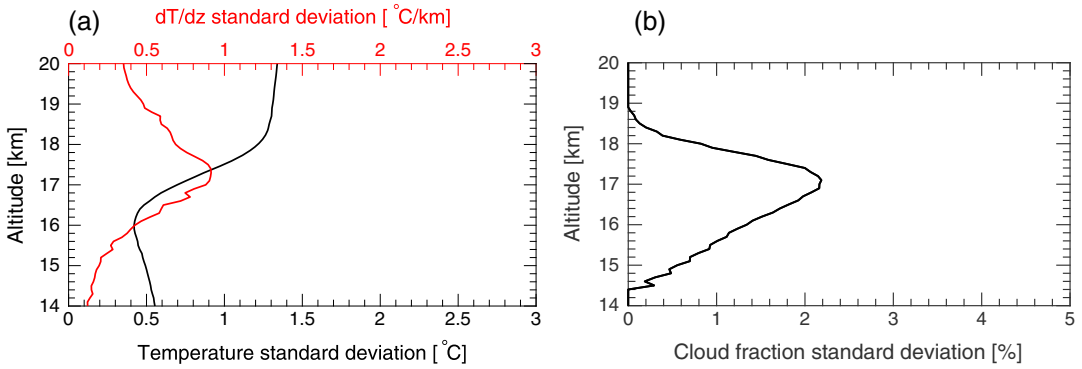

Figure 3. The same as Figure 2 but due to the interannual variability.

3.2. Vertical Profiles of Temporal Correlation Between TTL Cloud and Temperature-Based Variables

In order to quantify to what extent that the TTL cloud variation at different altitude is related to the temperature and temperature-based variables, Figures 6a and 7a show the vertical profiles of correlation coefficients between the TTL cloud fraction and four temperature-based variables for seasonal and interannual variations, respectively. The results are presented for the altitude from 14.5 km to 18.5 km where the TTL clouds occur (Figure 1b) (Fu et al., 2007). The correlation coefficient that exceeds the 95% confidence level, with the autocorrelation being taken into account (Bretherton et al., 1999), is denoted by filled circle.

The black lines in Figures 6a and 7a are the correlation coefficients between the TTL cloud fraction and temperature at the same altitude. It reaches a maximum negative value of −0.97 (−0.66) at ~16.4 km (~17.7 km) for the seasonal (interannual) variations. This correlation is low in the lower part of the TTL for both seasonal and interannual variations. The blue lines in Figures 6a and 7a are the correlation coefficients between the TTL clouds and vertical temperature gradient at the same altitude. The blue lines reach a maximum negative value of −0.98 (−0.8) at ~16.2 km (~16.9 km) for the seasonal (interannual) variations. The TTL cloud fraction is better correlated with the vertical temperature gradient than temperature below 16.6 km (17.6 km) for the seasonal (interannual) variations, while the opposite occurs above. Figures 6a and 7a show consistently high correlation coefficients (exceeding the 95% confidence level) between TTL cloud fraction and vertical temperature gradient below 17.5 km where most TTL clouds and their variability occur (Figures 1b, 2b, and 3b), consistent with Figures 4d and 5d.

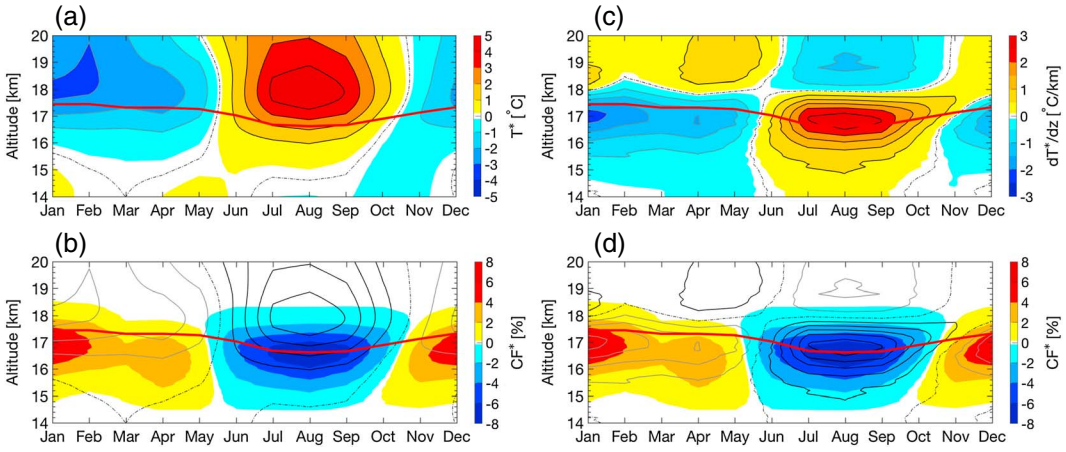

Figure 4. Seasonal variability of (a) COSMIC temperature (*T**), (b) CALIPSO TTL cloud fraction (CF*) along with the *T** contours, (c) COSMIC vertical temperature gradient (d*T**/dz), and (d) CF* with the contours of d*T**/dz, averaged over 15°N–15°S, as a function of month and height. The seasonal variability (i.e., the climatological mean seasonal cycle after removing the climatological annual mean value) is derived from the observations from June 2006 to April 2014. The red line is the climatological mean seasonal cycle of the COSMIC cold point tropopause height averaged over 15°N–15°S. The dashed line is zero line, while the solid black and solid gray lines are positive and negative values, respectively. The contour intervals are 1°C and 0.5°C/km for *T** and d*T**/dz, respectively. For color shading, the values near zero are represented by the white color.

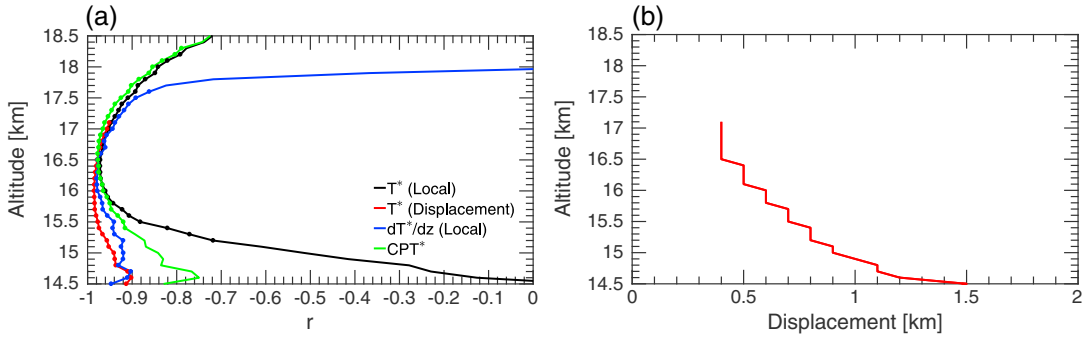

Figure 6. (a) Vertical profiles of correlation coefficient (*r*) between seasonal variations of TTL cloud fraction (CF*) and four temperature-based variables from observations for June 2006 to April 2014, averaged over 15°S–15°N. Correlation coefficient *r* that exceeds the 95% confidence level, with autocorrelation being taken into account (Bretherton et al., 1999), is denoted by filled circle. Shown are the correlation coefficients between CF* and *T** at the same altitude (black line), CF* and d*T**/d*z* at the same altitude (blue line), and CF* and the cold point tropopause temperature (CPT*) (green line). Red line shows the best correlation that is found by correlating CF* at a given level to the temperature above or below. (b) The corresponding vertical displacement for *T** to be best correlated with CF* at a given altitude. The positive displacement indicates that the best correlation is for CF* at a given altitude with *T** at a higher altitude.

and temperature-based variables. The first plausible mechanism is that the TTL clouds might form primarily near the tropopause and then sediment over time, as evidenced by the black, red, and green lines in Figures 6 and 7 (E. Jensen, personal communication, 2017). The black lines show that the TTL cloud variations are largely coherent with the same altitude temperature variation around the tropopause, while the clouds at lower part of the TTL are not. The red lines indicate that the TTL clouds are strongly correlated with the temperature at the higher altitude and the displacement increases with a decrease of height. The green lines, showing significant correlations at the 95% confidence level between the TTL clouds throughout the TTL with the CPT temperature, also indicate that the TTL clouds at all altitude are influenced by the temperature around the tropopause.

The second plausible mechanism is the cooling associated with wave propagation. By comparing the black and blue lines in Figures 6a and 7a (both are local correlation), the TTL cloud is better correlated with the vertical temperature gradient than temperature below around tropopause but vice versa above. Following a typical wave anomaly structure in the TTL, Kim, Alexander et al. (2016) suggested that vertical slope of the temperature anomaly has the same sign as its time derivative, and thus, the TTL cirrus clouds preferentially exist when a local air parcel experiences a cooling induced by wave. Our results (Figures 4d and 5d and blue lines in Figures 6a and 7a) are consistent with Kim, Alexander et al. (2016) although it is important to notice that in situ cloud ice and temperature measurements in Kim, Alexander et al. (2016) were truly coincident in space and time. Figure 6a (Figure 7a) shows that the cirrus variations are more related to the temperature than vertical temperature gradient above 16.5 km (17.5 km) for the seasonal (interannual) variations. This could be explained by the vertical dependence of the background relative humidity (RH_i), which is relatively high below the mean cold point tropopause but not above (Fueglistaler et al., 2009). A large cold temperature anomaly thus becomes critical for the TTL cloud formation/maintenance above the mean tropopause where the mean RH_i is low. On the other hand, the TTL cloud formation/maintenance

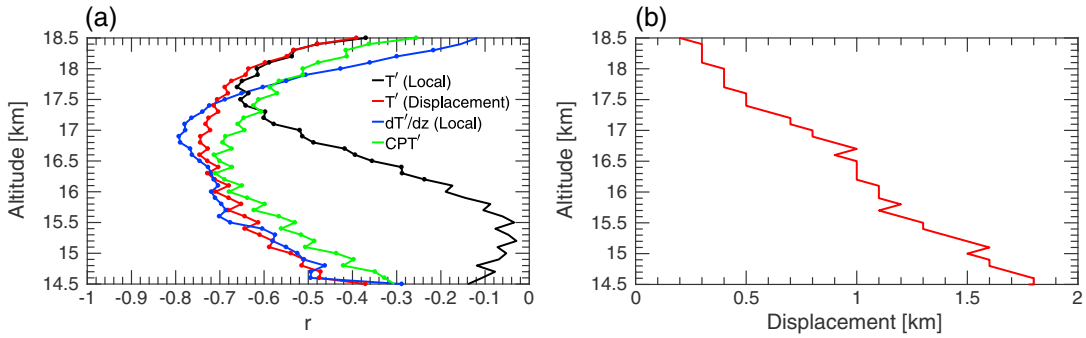

Figure 7. The same as Figure 6 but for the interannual variability.

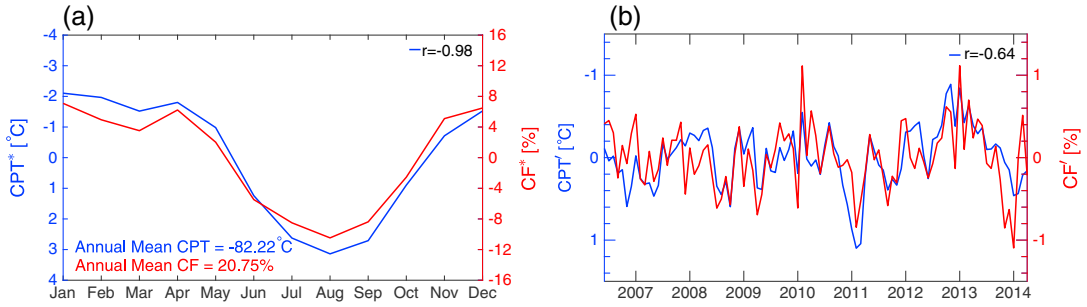

Figure 8. The (a) seasonal and (b) interannual variations of cold point tropopause temperature (CPT) (blue, with inverted scale) and TTL cloud fraction (CF) (red) averaged over 15°S–15°N for June 2006 to April 2014. The correlation coefficient (*r*) is shown in the upper right corner of each panel.

might just require a cooling when RH_i is close to saturation below the mean tropopause. Kim, Alexander et al. (2016) found by analyzing aircraft in situ observations that cirrus was more coincident with cold temperature anomalies above ~16.5 km. Boehm and Verlinde (2000) based on the ground-based lidar and radiosonde observations showed that cloud occurrences above 15 km usually coincide with cold temperature anomalies. The result from Boehm and Verlinde (2000) is not inconsistent with the present study that shows significant negative correlations between cirrus cloud fraction and local temperature above 15.2 km (16.2 km) for seasonal (interannual) variations (Figures 6a and 7a).

The third mechanism is the change of atmospheric stability. The blue lines in Figures 6a and 7a can be considered as the stability change instead. A negative vertical gradient of temperature anomaly indicates a more unstable environment, which would favor the cloud occurrence. On the other hand, the mean temperature increases with height above the mean tropopause, where a negative vertical gradient of temperature anomaly is not enough to induce upwelling.

The fourth mechanism is associated with the vertical gradient of saturated water vapor mixing ratio in clouds. The modeling study by Dinh et al. (2010) suggested that the key process to the maintenance of the TTL clouds is the circulation thermally forced by the cloud radiative heating. They showed that the circulation is advected horizontally toward the center of the cloud bottom and then move vertically upward once it is inside the cloud. When the cloud layer is at ice saturation and temperature decreases with height, the saturated water vapor mixing ratio decreases with height, resulting in water vapor flux convergence and ice growth by the thermally forced circulation. Therefore, a negative vertical gradient of temperature anomaly that leads to a larger water vapor mixing ratio vertical gradient would favor the TTL cloud maintenance for clouds below the tropopause where temperature decreases with height.

Furthermore, the radiative heating of TTL clouds might also affect the observed temperature and vertical temperature gradient. While here we discuss several plausible mechanisms that might be responsible for the observed relations between the TTL clouds and temperature-based variables, it will be our future research effort to validate/exclude these mechanisms and examine their relative roles including the role of the TTL cloud radiative feedback.

4. Spatial Covariability Between the TTL Clouds and Tropopause Temperature

The results in section 3 indicate that the CPT temperature can well represent the role of the TTL temperature in influencing the TTL clouds. Here we investigate the spatial covariability of the CPT temperature with the total TTL cloud fraction on the interannual time scale. We apply maximum covariance analysis (MCA) (Wallace et al., 1992) to the deseasonalized monthly gridded CPT temperature and total TTL cloud fraction to identify the coupling patterns between the two fields. We will then explore the relation of these patterns to the large-scale dynamic variability including ENSO, QBO, BDC, and MJO.

Displayed in Figure 9 is the spatial covariability of the monthly gridded (5° latitude by 10° longitude) TTL total cloud fraction anomaly and CPT temperature anomaly over the whole tropics (30°S–30°N). The MCA leading mode (MCA1) explains 57% of the covariance. The MCA1 patterns shows that the spatial variation of TTL clouds is primarily govern by the oscillation of TTL temperature between the western Pacific and the central to the eastern Pacific, which is an ENSO-like dipole pattern. The correlation coefficient between the

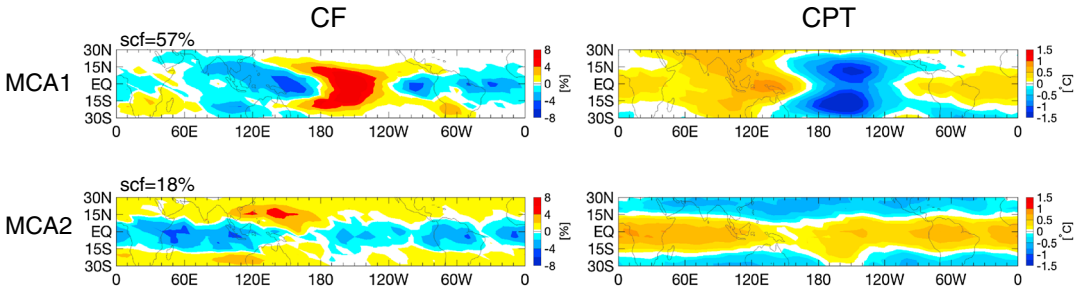

Figure 9. Coupled patterns between the (left column) TTL cloud fraction and (right column) tropical CPT temperature for June 2006 to April 2014 from the maximum covariance analysis (MCA) applied to the deseasonalized monthly tropical (30°S–30°N) gridded TTL total cloud fraction and CPT temperature. (first and second rows) The coupled patterns that accompany the first and second modes, respectively. The squared covariance fraction is shown above the upper left of each CF panel for color shading; the values near 0 are represented by the white color.

corresponding two MCA1 time series is 0.95. The MCA second mode (MCA2) accounts for 18% of the covariance. The MCA2 patterns indicate that temperature in this mode affect the TTL clouds mainly in the deep tropics. The correlation coefficient between the two MCA2 time series is 0.89. The MCA third mode (MCA3) (not shown) plays a relatively minor role, which explains 8% of the covariance. The MCA3 also shows the dipole variability for both fields and the correlation between the two corresponding MCA3 time series is 0.89.

We examine the role of the large-scale dynamical variability in controlling the temperature and cloud variations in the TTL. Figures 10a and 10b show the spatial distribution of the correlation between deseasonalized monthly tropical (30°S–30°N) gridded TTL total cloud fraction (left) and CPT (right) temperature, to the ENSO and QBO indices, respectively, for June 2006 to April 2014. The correlation spatial patterns with the ENSO (Figures 10a and 10b) and QBO (Figures 10c and 10d) highly resemble the coupled patterns of MCA1 and MCA2 (Figure 9), respectively. This indicates that the coupled patterns of MCA1 (MCA2) are largely controlled by the ENSO (QBO).

We further quantify the relation between the MCA three leading modes and the large-scale dynamic variability of ENSO, QBO, BDC, and MJO. Figure 11a shows that both time series from MCA1 are highly correlated with ENSO ($r = 0.83$ for the cloud fraction and 0.86 for the CPT temperature). The two MCA2 time series are strongly correlated with QBO index ($r = 0.5$ and 0.62) (Figure 11b). We also examine the correlations between MCA3 time series and BDC index and MJO index. It is obtained that $r = 0.14$ for BDC and CF and 0.06 for BDC and CPT, which are both not significant at the 95% confidence level. But we have $r = -0.21$ for MJO and CF and -0.27 for MJO and CPT when using the second-principle component of MJO index, which are both statistically significant. MCA3 mode might also be affected by other large-scale dynamical variability (Ding & Fu, 2017). Overall, it is suggested that ENSO and QBO are the leading factors in controlling the spatial variability of the TTL cirrus clouds and temperatures. It is interesting to notice that the ENSO, QBO, and MJO indices are only significantly correlated with the principle components (for both TTL cloud fraction and CPT) from MCA1,

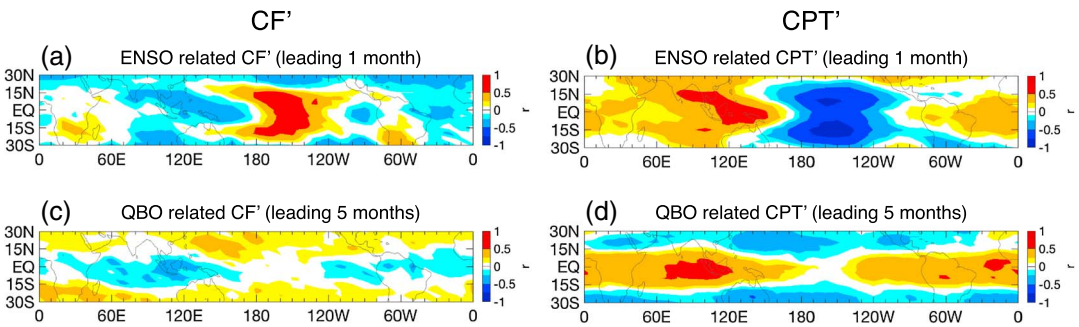

Figure 10. Correlation maps of deseasonalized monthly tropical (30°S–30°N) gridded (a and c) TTL total cloud fraction and (b and d) CPT temperature to the ENSO (Figures 10a and 10b) and QBO (Figures 10b and 10d) indices for June 2006 to April 2014, with the ENSO and QBO leading by 1 and 5 months, respectively, to obtain the best correlations. For color shading, the values near 0 are represented by the white color.

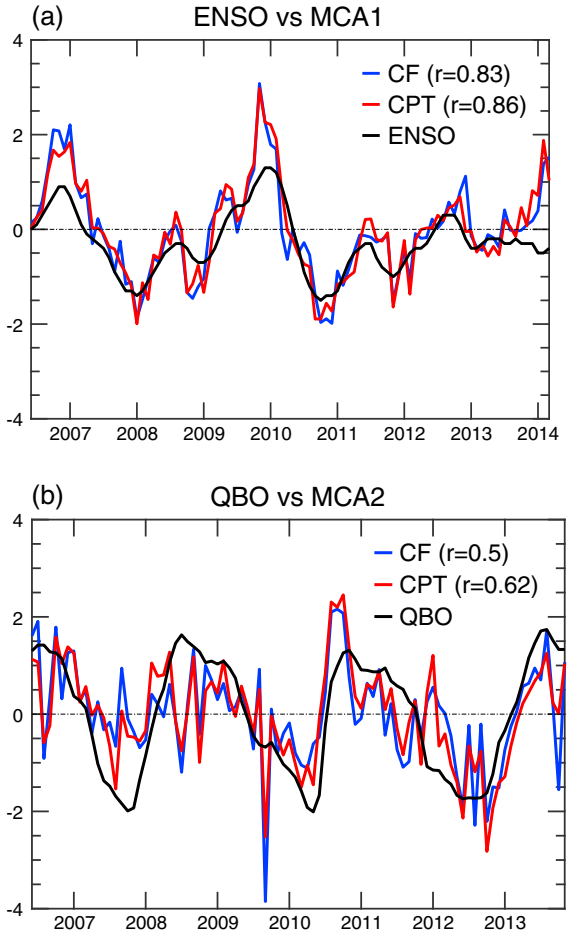

Figure 11. The time series of the coupled patterns (Figure 9) of the TTL total cloud (blue) and CPT temperature (red) from the MCA for the (a) mode 1 along with the ENSO index (black) and (b) mode 2 along with the QBO index (black). The time axis of the time series of the TTL cloud fraction and CPT temperature is shifted by 1 and 5 months to align with those of the ENSO and QBO in Figures 11a and 11b, respectively. The correlation coefficient (*r*) of the MCA time series with climate index is shown in parentheses.

MCA2, and MCA3, respectively. The BDC index is not significantly correlated with any principle components of these three MCA modes.

Davis et al. (2013) computed the empirical orthogonal functions (EOFs) of the 100 hPa temperatures from the Modern-Era Retrospective Analysis for Research and Applications reanalysis and TTL cloud fraction between 16 and 17 km from the CALIPSO observations. Their leading EOF spatial patterns are very similar to the MCA1 patterns for both cloud fraction and temperatures (Figure 9), with the principle components highly correlated with the ENSO index (0.85 for temperature and 0.81 for clouds) (see their Figure 3). However, their second EOF patterns for temperatures and clouds are less consistent with each other than those of MCA2, with the second EOF pattern similar to MCA2 for clouds but not for temperatures. This is caused by different methods used to analyze the data, that is, EOF versus MCA. Very different from our results shown in Figure 10, their second EOF principle components are highly correlated with their BDC index (0.66 for temperature and 0.59 for clouds). Davis et al. (2013) showed that the QBO plays little role in determining the spatial distribution of TTL clouds (the correlation coefficient between the QBO index and their third EOF principle component is only 0.07). The differences between our results and those in Davis et al. (2013) are mainly because they used the total heating rate anomaly at 82 hPa as a measure of the BDC, which already includes the QBO contributions (Yang et al., 2008). The differences are also partly caused by the different methods used, that is, EOF versus MCA, as discussed above. Davis et al. (2013) did not consider the role of the MJO.

In terms of the TTL total cloud fraction and temperatures averaged over 15°N and 15°S, we apply the multiple regressions to relate them to the ENSO, QBO, BDC, and MJO indices. It is found that QBO (BDC) can explain 16.7% (6.7%) of the CF′ variance and 33.4% (23.4%) of the CPT′ variance, while ENSO (MJO) can only explain 3.7% (3.0%) of the CF′ variance and 0.6% (0.8%) of the CPT′ variance. Thus, QBO and BDC signals are much more dominant than ENSO and MJO for the zonal mean variability. This is because the spatial positive and negative signals associated with ENSO are largely canceled out (Figures 10a and 10b) (also see Davis et al., 2013). This is also true for MJO signal as indicated by the MCA3 (not shown). Li and Thompson (2013) also found a significant linkage between the BDC and zonal TTL clouds on month-to-month time scales but for the NH winter months only (October–March) based on anomalous data.

Davis et al. (2013) showed that the interannual variability of the TTL cloud and temperature averaged in the deep tropics is related to both QBO and BDC by presenting significant correlations of these indices with the TTL clouds and temperatures. Their results are expected if the QBO is the main factor controlling the zonal mean TTL variability since their BDC index contains the QBO signal. In contrast, our QBO and BDC indices are independent of each other. Our results therefore really show that both QBO and BDC are important in determining the zonal mean variability of the TTL clouds and temperatures (we further examine their relative roles using the multiple regressions).

Finally, we have also carried out the MCA for the TTL cloud fraction and temperature anomalies at the same given level for multiple altitudes throughout the TTL (not shown). It is found that the QBO becomes the dominant factor and ENSO becomes the second above 17.5 km in determining the spatial covariability of the TTL cloud fraction and temperatures.

5. Discussion and Conclusions

The TTL cirrus cloud and its relationship with temperature are investigated by using 8 years of CALIPSO and COSMIC observations. We find that (i) the temporal variation of the TTL cloud fraction vertical structure averaged between 15°N and 15°S can be well explained by the vertical temperature gradient below ~17.5 km but by the local temperature above for both the seasonal and interannual time scales; (ii) the TTL cloud fraction at a given altitude is best correlated with the temperature at a higher altitude and this displacement increases with a decrease of cirrus height; (iii) the TTL cloud fractions at all altitudes are significantly correlated with CPT temperature; and (iv) the correlation coefficients of TTL cloud fractions with the temperature-based variables all reach the maxima around 16.5–17.5 km.

We discuss four plausible mechanisms that could be responsible for the observed relations between TTL cirrus and the temperature-based variables, which include ice particle sediments, cooling related to the large-scale wave propagations, atmospheric stability change, and water vapor mixing ratio vertical gradient. Whether these mechanisms are correct and to what extent they are important and what their relative roles are require future research.

We further examine the spatial covariability of the TTL total cloud fraction and cold point tropopause temperature by using MCA over the entire tropics (30°S–30°N). It is shown that the ENSO is the first leading factor and the QBO is the second in controlling the spatial variability of the TTL cirrus clouds and temperatures. But the QBO and BDC becomes the first and second dominant factors to determine the variability of the TTL total cloud fraction and temperatures averaged over 15°N and 15°S where the spatial positive and negative signals associated with ENSO and MJO are largely canceled out.

Acknowledgments

We thank Dale Durran for the suggestion on the mechanism associated with the vertical gradient of water vapor mixing ratio. We thank Eric Jensen, Mike Wallace, William Randel, Stephan Fueglistaler, and Rei Ueyama for their encouragements and helpful suggestions on this work. This research was supported by NASA grant NNX16AO95G. The CALIPSO data are from the NASA Langley Research Center Atmospheric Sciences Data Center. The COSMIC data are obtained through the COSMIC Data Analysis and Archive Center, operated by UCAR/COSMIC program. The ENSO index is from the NOAA Climate Prediction Center. The QBO data set is from Department of Earth Sciences of the Freie Universität Berlin. The BDC index that calculated from the ERA-interim data is from European Centre for Medium-Range Weather Forecasts. The MJO index is obtained from NOAA Earth System Research Laboratory, Physical Sciences Division. All observational results are stored in the University of Washington Research Works Archive (http://hdl.handle.net/1773/40318).

References

Alcala, C., & Dessler, A. (2002). Observations of deep convection in the tropics using the Tropical Rainfall Measuring Mission (TRMM) precipitation radar. *Journal of Geophysical Research*, *107*(D24), 4792. https://doi.org/10.1029/2002JD002457

Anthes, R. A., Bernhardt, P., Chen, Y., Cucurull, L., Dymond, K., Ector, D., … Yen, N. L. (2008). The COSMIC/FORMOSAT-3 mission: Early results. *Bulletin of the American Meteorological Society*, *89*(3), 313–333.

Bethan, S., Vaughan, G., & Reid, S. (1996). A comparison of ozone and thermal tropopause heights and the impact of tropopause definition on quantifying the ozone content of the troposphere. *Quarterly Journal of the Royal Meteorological Society*, *122*(532), 929–944.

Boehm, M. T., & Verlinde, J. (2000). Stratospheric influence on upper tropospheric tropical cirrus. *Geophysical Research Letters*, *27*(19), 3209–3212. https://doi.org/10.1029/2000GL011678

Brasseur, G. P., & Solomon, S. (2006). *Aeronomy of the middle atmosphere: Chemistry and physics of the stratosphere and mesosphere* (Vol. 32). Netherlands: Springer Science and Business Media.

Bretherton, C. S., Widmann, M., Dymnikov, V. P., Wallace, J. M., & Bladé, I. (1999). The effective number of spatial degrees of freedom of a time-varying field. *Journal of Climate*, *12*(7), 1990–2009.

Brewer, A. (1949). Evidence for a world circulation provided by the measurements of helium and water vapour distribution in the stratosphere. *Quarterly Journal of the Royal Meteorological Society*, *75*(326), 351–363.

Comstock, J. M., Ackerman, T. P., & Mace, G. G. (2002). Ground-based lidar and radar re- mote sensing of tropical cirrus clouds at Nauru Island: Cloud statistics and radiative impacts. *Journal of Geophysical Research*, *107*(D23), 4714, AAC 16-1–AAC 16-14. https://doi.org/10.1029/2002JD002203

Corti, T., Luo, B., Fu, Q., Vömel, H., & Peter, T. (2006). The impact of cirrus clouds on tropical troposphere-to-stratosphere transport. *Atmospheric Chemistry and Physics*, *6*(9), 2539–2547.

Corti, T., Luo, B. P., Peter, T., Vömel, H., & Fu, Q. (2005). Mean radiative energy balance and vertical mass fluxes in the equatorial upper troposphere and lower stratosphere. *Geophysical Research Letters*, *32*, L06802. https://doi.org/10.1029/2004GL021889

Davis, S. M., Liang, C. K., & Rosenlof, K. H. (2013). Interannual variability of tropical tropopause layer clouds. *Geophysical Research Letters*, *40*(11), 2862–2866. https://doi.org/10.1002/grl.50512

Dee, D., Uppala, S., Simmons, A., Berrisford, P., Poli, P., Kobayashi, S., … Vitart, F. (2011). The ERA-interim reanalysis: Configuration and performance of the data assimilation system. *Quarterly Journal of the Royal Meteorological Society*, *137*(656), 553–597.

Ding, Q., & Fu, Q. (2017). A warming tropical central Pacific dries the lower stratosphere. *Climate Dynamics*, 1–15.

Dinh, T. P., Durran, D., & Ackerman, T. (2010). Maintenance of tropical tropopause layer cirrus. *Journal of Geophysical Research*, *115*, D02104. https://doi.org/10.1029/2009JD012735

Dobson, G. (1956). Origin and distribution of the polyatomic molecules in the atmosphere. *Proceedings of the Royal Society of London. Series A: Mathematical and Physical Sciences*, *236*(1205), 187–193.

Folkins, I., Loewenstein, M., Podolske, J., Oltmans, S. J., & Proffitt, M. (1999). A barrier to vertical mixing at 14 km in the tropics: Evidence from ozonesondes and aircraft measurements. *Journal of Geophysical Research*, *104*(D18), 22,095–22,102. https://doi.org/10.1029/1999JD900404

Fu, Q. (2013). Bottom up in the tropics. *Nature Climate Change*, *3*(11), 957–958.

Fu, Q., Hu, Y., & Yang, Q. (2007). Identifying the top of the tropical tropopause layer from vertical mass flux analysis and CALIPSO lidar cloud observations. *Geophysical Research Letters*, *34*, L14813. https://doi.org/10.1029/2007GL030099

Fueglistaler, S., Dessler, A., Dunkerton, T., Folkins, I., Fu, Q., & Mote, P. W. (2009). Tropical tropopause layer. *Reviews of Geophysics*, *47*, RG1004. https://doi.org/10.1029/2008RG000267

Fueglistaler, S., & Fu, Q. (2006). Impact of clouds on radiative heating rates in the tropical lower stratosphere. *Journal of Geophysical Research*, *111*, D23202. https://doi.org/10.1029/2006JD007273

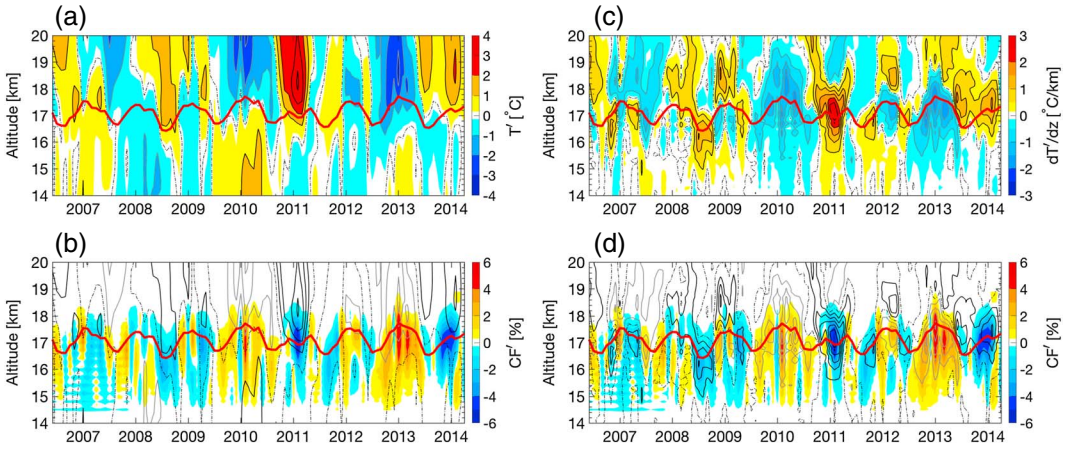

Figure 5. The same as Figure 4 but for the interannual variability. The monthly anomalies for the temperature (T') and cloud fraction (CF′) are derived by removing the climatological mean seasonal cycle. The red line is the monthly mean COSMIC cold point tropopause height averaged over 15°S–15°N. The contour intervals are 1°C and 0.5°C/km for T' and dT'/dz, respectively. For color shading, the values near zero are represented by the white color.

The red lines in Figures 6a and 7a are the correlation coefficients between the TTL cloud fraction at given level and temperature at the level with a displacement to reach the best correlation. The corresponding displacement (i.e., the temperature height minus the cloud height) is shown in Figures 6b and 7b. The TTL cloud fraction at a given level is always best correlated with temperature at a higher altitude, and the displacement increases with a decrease of the cloud altitude. Comparing the blue line with red line in Figures 6a and 7a, the correlation between the TTL cloud fraction and vertical temperature gradient below the tropopause is very similar to the best correlation between the TTL cloud fraction and temperature with a displacement.

The green lines in Figures 6a and 7a show the correlation coefficient of the cold point tropopause (CPT) temperature with the TTL cloud fraction at different altitudes throughout the TTL. It shows significant correlations at the 95% confidence level throughout the TTL for the interannual variability although the correlation from the green line is not as high as the red line (Figure 7a). Figures 6a and 7a indicate that the correlation coefficients of TTL cloud fractions with the temperature-based variables all reach the maxima around ~16.5 to 17.5 km.

Figure 8 shows the seasonal and interannual variations of the CPT temperature and the total TTL cloud fraction that is for all clouds with cloud bases higher than 14.5 km. The correlation coefficients are −0.98 and −0.64 for seasonal and interannual variations, respectively, which are both significant at the 95% confidence level. It is interesting to note that intraseasonal variations of the CPT temperature and TTL cloud fraction are also highly correlated (−0.61), as shown by Virts et al. (2010) who applied 80 day high-pass filter to the data at a tropical site. Figures 6a, 7a, and 8 indicate that the CPT temperature can reasonably represent the role of the TTL temperature in controlling the TTL clouds.

3.3. Plausible Mechanisms

Herein, we continue our discussions on the results presented in sections 3.1 and 3.2 by offering a few plausible mechanisms that could be (partly) responsible for the observed relations between the TTL clouds

Table 1
The Occurrence Frequency of Positive and Negative TTL Cloud Fraction Variability (i.e., CF and CF′) on Both Seasonal (Upper) and Interannual (Lower) Time Scales Under Four Conditions Based On the Sign of the Variability in Temperature (i.e., T* and T′) and Vertical Temperature Gradient (i.e., dT*/dz and dT′/dz) Between 14.5 km and 20 km*

		Seasonal		
CF*	$T^* < 0$ and $dT^*/dz < 0$	$T^* < 0$ and $dT^*/dz > 0$	$T^* > 0$ and $dT^*/dz < 0$	$T^* > 0$ and $dT^*/dz > 0$
CF* > 0	72.0%	12.4%	15.3%	0.3%
CF* < 0	1.9%	22.6%	7.1%	68.4%
		Interannual		
CF′	$T' < 0$ and $dT'/dz < 0$	$T' < 0$ and $dT'/dz > 0$	$T' > 0$ and $dT'/dz < 0$	$T' > 0$ and $dT'/dz > 0$
CF′ > 0	45.7%	18.9%	27%	8.4%
CF′ < 0	11.8%	30.1%	16.3%	41.8%

Fueglistaler, S., & Haynes, P. H. (2005). Control of interannual and longer-term variability of stratospheric water vapor. *Journal of Geophysical Research*, *110*, D24108. https://doi.org/10.1029/2005JD006019

Gettelman, A., & Forster, P. D. F. (2002). A climatology of the tropical tropopause layer. *Journal of the Meteorological Society of Japan*, *80*(4B), 911–924.

Gettelman, A., Forster, P. M. D. F., Fujiwara, M., Fu, Q., Vömel, H., Gohar, L. K., … Ammerman, M. (2004). Radiation balance of the tropical tropopause layer. *Journal of Geophysical Research*, *109*, D07103. https://doi.org/10.1029/2003JD004190

Grise, K. M., & Thompson, D. W. (2013). On the signatures of equatorial and extratropical wave forcing in tropical tropopause layer temperatures. *Journal of the Atmospheric Sciences*, *70*(4), 1084–1102.

Hajj, G. A., Ao, C., Iijima, B., Kuang, D., Kursinski, E., Mannucci, A., … Yunck, T. (2004). Champ and SAC-C atmospheric occultation results and intercomparisons. *Journal of Geophysical Research*, *109*, D06109. https://doi.org/10.1029/2003JD003909

He, W., Ho, S.-P., Chen, H., Zhou, X., Hunt, D., & Kuo, Y.-H. (2009). Assessment of radiosonde temperature measurements in the upper troposphere and lower stratosphere using COSMIC radio occultation data. *Geophysical Research Letters*, *36*, L17807. https://doi.org/10.1029/2009GL038712

Held, I. M., & Hoskins, B. J. (1985). Large-scale eddies and the general circulation of the troposphere. *Advances in Geophysics*, *28*, 3–31.

Highwood, E., & Hoskins, B. (1998). The tropical tropopause. *Quarterly Journal of the Royal Meteorological Society*, *124*(549), 1579–1604.

Holton, J. R., & Gettelman, A. (2001). Horizontal transport and the dehydration of the stratosphere. *Geophysical Research Letters*, *28*(14), 2799–2802. https://doi.org/10.1029/2001GL013148

Holton, J. R., Haynes, P. H., McIntyre, M. E., Douglass, A. R., Rood, R. B., & Pfister, L. (1995). Stratosphere-troposphere exchange. *Reviews of Geophysics*, *33*(4), 403–439. https://doi.org/10.1029/95RG02097

Hu, Y., & Tung, K. K. (2002). Interannual and decadal variations of planetary wave activity, stratospheric cooling, and Northern Hemisphere annular mode. *Journal of Climate*, *15*(13), 1659–1673.

Jensen, E. J., Toon, O. B., Selkirk, H. B., Spinhirne, J. D., & Schoeberl, M. R. (1996). On the formation and persistence of subvisible cirrus clouds near the tropical tropopause. *Journal of Geophysical Research*, *101*(D16), 21,361–21,375.

Kerr-Munslow, A., & Norton, W. (2006). Tropical wave driving of the annual cycle in tropical tropopause temperatures. Part I: ECMWF analyses. *Journal of the Atmospheric Sciences*, *63*(5), 1410–1419.

Kim, J., Randel, W. J., Birner, T., & Abalos, M. (2016). Spectrum of wave forcing associated with the annual cycle of upwelling at the tropical tropopause. *Journal of the Atmospheric Sciences*, *73*(2), 855–868.

Kim, J.-E., Alexander, M. J., Bui, T. P., Dean-Day, J. M., Lawson, R. P., Woods, S., … Jensen, E. J. (2016). Ubiquitous influence of waves on tropical high cirrus clouds. *Geophysical Research Letters*, *43*(11), 5895–5901. https://doi.org/10.1002/2016GL069293

Kuo, Y.-H., Wee, T.-K., Sokolovskiy, S., Rocken, C., Schreiner, W., Hunt, D., & Anthes, R. (2004). Inversion and error estimation of GPS radio occultation data. *Journal of the Meteorological Society of Japan*, *82*(1B), 507–531.

Kursinski, E., Hajj, G., Schofield, J., Linfield, R., & Hardy, K. R. (1997). Observing Earth's atmosphere with radio occultation measurements using the Global Positioning System. *Journal of Geophysical Research*, *102*(D19), 23,429–23,465.

Li, Y., & Thompson, D. W. (2013). The signature of the stratospheric brewer-Dobson circulation in tropospheric clouds. *Journal of Geophysical Research: Atmospheres*, *118*(9), 3486–3494. https://doi.org/10.1002/jgrd.50339

Lin, L., Fu, Q., Zhang, H., Su, J., Yang, Q., & Sun, Z. (2013). Upward mass fluxes in tropical upper troposphere and lower stratosphere derived from radiative transfer calculations. *Journal of Quantitative Spectroscopy and Radiative Transfer*, *117*, 114–122.

Lin, P., Fu, Q., Solomon, S., & Wallace, J. M. (2009). Temperature trend patterns in Southern Hemisphere high latitudes: Novel indicators of stratospheric change. *Journal of Climate*, *22*(23), 6325–6341.

Norton, W. (2006). Tropical wave driving of the annual cycle in tropical tropopause temperatures. Part II: Model results. *Journal of the Atmospheric Sciences*, *63*(5), 1420–1431.

Randel, W. J., Garcia, R., & Wu, F. (2008). Dynamical balances and tropical stratospheric upwelling. *Journal of the Atmospheric Sciences*, *65*(11), 3584–3595.

Randel, W. J., Garcia, R. R., & Wu, F. (2002). Time-dependent upwelling in the tropical lower stratosphere estimated from the zonal-mean momentum budget. *Journal of the Atmospheric Sciences*, *59*(13), 2141–2152.

Randel, W. J., & Wu, F. (2015). Variability of zonal mean tropical temperatures derived from a decade of GPS radio occultation data. *Journal of the Atmospheric Sciences*, *72*(3), 1261–1275.

Rosenhof, K. H. (1995). Seasonal cycle of the residual mean meridional circulation in the stratosphere. *Journal of Geophysical Research*, *100*(D3), 5173–5191.

Sherwood, S. C., & Dessler, A. E. (2000). On the control of stratospheric humidity. *Geophysical Research Letters*, *27*(16), 2513–2516.

Solomon, S., Rosenlof, K. H., Portmann, R. W., Daniel, J. S., Davis, S. M., Sanford, T. J., & Plattner, G.-K. (2010). Contributions of stratospheric water vapor to decadal changes in the rate of global warming. *Science*, *327*(5970), 1219–1223.

Son, S.-W., Tandon, N. F., & Polvani, L. M. (2011). The fine-scale structure of the global tropopause derived from COSMIC GPS radio occultation measurements. *Journal of Geophysical Research*, *116*, D20113. https://doi.org/10.1029/2011JD016030

Sun, B., Reale, A., Seidel, D. J., & Hunt, D. C. (2010). Comparing radiosonde and COSMIC atmospheric profile data to quantify differences among radiosonde types and the effects of imperfect collocation on comparison statistics. *Journal of Geophysical Research*, *115*, D23104. https://doi.org/10.1029/2010JD014457

Taylor, J. R., Randel, W. J., & Jensen, E. J. (2011). Cirrus cloud-temperature interactions in the tropical tropopause layer: A case study. *Atmospheric Chemistry and Physics*, *11*(19), 10,085–10,095.

Tseng, H.-H., & Fu, Q. (2017). Tropical tropopause layer cirrus and its relation to tropopause. *Journal of Quantitative Spectroscopy and Radiative Transfer*, *188*, 118–131.

Tuck, A., Baumgardner, D., Chan, K., Dye, J., Elkins, J., Hovde, S., … Wilson, J. C. (1997). The Brewer-Dobson circulation in the light of high altitude in situ aircraft observations. *Quarterly Journal of the Royal Meteorological Society*, *123*(537), 1–69.

Ueyama, R., & Wallace, J. M. (2010). To what extent does high-latitude wave forcing drive tropical upwelling in the Brewer-Dobson circulation? *Journal of the Atmospheric Sciences*, *67*(4), 1232–1246.

Vaughan, M. A., Powell, K. A., Winker, D. M., Hostetler, C. A., Kuehn, R. E., Hunt, W. H., … McGill, M. J. (2009). Fully automated detection of cloud and aerosol layers in the CALIPSO lidar measurements. *Journal of Atmospheric and Oceanic Technology*, *26*(10), 2034–2050.

Ventrice, M. J., Wheeler, M. C., Hendon, H. H., Schreck, C. J. III, Thorncroft, C. D., & Kiladis, G. N. (2013). A modified multivariate Madden–Julian oscillation index using velocity potential. *Monthly Weather Review*, *141*(12), 4197–4210.

Virts, K. S., & Wallace, J. M. (2010). Annual, interannual, and intraseasonal variability of tropical tropopause transition layer cirrus. *Journal of the Atmospheric Sciences*, *67*(10), 3097–3112.

Virts, K. S., & Wallace, J. M. (2014). Observations of temperature, wind, cirrus, and trace gases in the tropical tropopause transition layer during the MJO. *Journal of the Atmospheric Sciences*, *71*(3), 1143–1157.

Virts, K. S., Wallace, J. M., Fu, Q., & Ackerman, T. P. (2010). Tropical tropopause transition layer cirrus as represented by CALIPSO lidar observations. *Journal of the Atmospheric Sciences*, *67*(10), 3113–3129.

Wallace, J. M., Smith, C., & Bretherton, C. S. (1992). Singular value decomposition of wintertime sea surface temperature and 500-mb height anomalies. *Journal of Climate*, *5*(6), 561–576.

Wheeler, M. C., & Hendon, H. H. (2004). An all-season real-time multivariate MJO index: Development of an index for monitoring and prediction. *Monthly Weather Review*, *132*(8), 1917–1932.

Winker, D., Pelon, J., Coakley, J. Jr., Ackerman, S., Charlson, R., Colarco, P., … Wielicki, B. A. (2010). The CALIPSO mission: A global 3D view of aerosols and clouds. *Bulletin of the American Meteorological Society*, *91*(9), 1211–1229.

Winker, D. M., Vaughan, M. A., Omar, A., Hu, Y., Powell, K. A., Liu, Z., … Young, S. A. (2009). Overview of the CALIPSO mission and CALIOP data processing algorithms. *Journal of Atmospheric and Oceanic Technology*, *26*(11), 2310–2323.

Yang, Q., Fu, Q., Austin, J., Gettelman, A., Li, F., & Vömel, H. (2008). Observationally derived and general circulation model simulated tropical stratospheric upward mass fluxes. *Journal of Geophysical Research*, *113*, D00B07. https://doi.org/10.1029/2008JD009945

Yang, Q., Fu, Q., & Hu, Y. (2010). Radiative impacts of clouds in the tropical tropopause layer. *Journal of Geophysical Research*, *115*, D00H12. https://doi.org/10.1029/2009JD012393

Yulaeva, E., Holton, J. R., & Wallace, J. M. (1994). On the cause of the annual cycle in tropical lower-stratospheric temperatures. *Journal of the Atmospheric Sciences*, *51*(2), 169–174.